Available online at www.sciencedirect.com
SCIENCE DIRECT®
International Journal of Solids and Structures 42 (2005) 1819–1830
INTERNATIONAL JOURNAL OF SOLIDS and STRUCTURES
www.elsevier.com/locate/ijsolstr

Bending of a simple beam to an optically accurate parabolic shape

Jason A. Tolomeo *

Lockheed Martin Advanced Technology Center, ABDS, 3251 Hanover St., Palo Alto, CA 94304, USA

Received 21 October 2003; received in revised form 10 August 2004
Available online 25 September 2004

Abstract

Ultra-lightweight optical imaging systems for space based applications are being developed where the primary optical surface is made of reflective stretched membrane material. In these systems, the supporting structure and the optical surface are highly interrelated. The first step in implementing such a precision large membrane optical system is accurately defining the boundary of the membrane area. In this paper, it is shown that a flat constant cross section beam can be elastically shaped to parabolic curvature to very high accuracy using a simple set of end moments and forces. The necessary design relationship between the applied loads are analytically derived for the geometric nonlinear case and shown to apply to a wide range of curvature and apertures sizes. The utility of the method is then demonstrated experimentally. The predicted RMS error from parabolic shape is proportional to the reflector F-number as $(F/\#)^{-4}$ for off-axis designs and $(F/\#)^{-5}$ for on-axis designs. This is a feasible and desirable method of forming parabolic boundary members for a range of electromagnetic wavelengths since the constant cross section initially flat beams can be scaled in design and fabrication to very large sizes. This method of forming boundary shape has particular application to Dual Anamorphic Reflector Telescope (DART) designs.

Keywords: Nonlinear beam; Lightweight optics; Gossamer; DART; Space telescope

1. Introduction

Precision optical systems require highly accurate surfaces on optical reflectors with deviations from ideal shape that must be small in comparison to the wavelength of light to be used. For visible wavelength based systems, this implies surface accuracy of about 30 nm spatial RMS. The concept of reflectors made from

* Tel.: +1 650 424 2242; fax: +1 650 354 5002.
E-mail address: jason.a.tolomeo@lmco.com

0020-7683/$ - see front matter © 2004 Elsevier Ltd. All rights reserved.
doi:10.1016/j.ijsolstr.2004.08.012

thin stretched membranes is currently an active area of research and development for space based optical systems. The potential advantages of membrane reflectors are reduced production time and cost, packaging and deployments to very large systems, and total mass. A significant difficulty with membrane reflector structures is achieving and maintaining the required surface accuracy.

State-of-the-art methods of achieving figure in light-weighted optics consist of many actuators beneath a thin reflector (Burge et al., 2000). Other methods of forming large rotationally symmetric optical membranes have been proposed, including boundary and interior moment control (Ash et al., 2000; Jenkins et al., 1998), pressurization (Rotge et al., 2000), and electrostatics (Dimakov et al., 2000). However, these proposed methods on circularly symmetric membrane mirrors have had difficulty in implementation and achieving accurate figure. The advantage of forming a parabolic boundary from flat constant cross-section beams is that they can be precisely manufactured and polished flat in a manner that is scalable to very large systems, on the order of 10's of meters in length. This is a significant advantage in development of membrane reflectors and is particularly suited to dual anamorphic reflector telescope (DART) systems.

In a dual anamorphic reflector system, a pair of orthogonally oriented single curvature membrane reflectors replace the role of a conventional double curvature primary mirror (Dragovan, 2002). Each of the single curvature mirrors is a cylindrical parabola. This substantially simplifies the task of forming the membrane reflector since a cylindrical parabola has zero Gaussian curvature, indicating that it can be formed directly from a flat sheet, without the need to impose local gradients of strain. The cylindrical parabolas are formed by stretching a membrane between two parabolic shaped edge boundaries. Stretching the membrane provides stiffness as well as propagates the boundary curvature throughout the interior surface of the membrane reflector. The task then is to accurately define the parabolic shape of two opposing edge boundaries so that the RMS deviation from parabolic shape is a small fraction of the wavelength of light to be reflected.

In this paper an analytical basis for bending precision flat constant cross section beams into highly accurate on-axis and off-axis parabolic edge boundary members is fully derived. The innovation of balancing a simple set of end loads and moments to produce a curved beam with quantitatively small error from parabolic shape has been previously described and experimentally verified at the optical system level (Tolomeo et al., 2002, patent pending). It has subsequently been further verified for a specific geometry using finite element techniques (White et al., 2003). Once the high precision rails are formed, the membrane can then be stretched between these beams in order to produce a cylindrical parabolic reflector.

The analysis begins with a treatment of the geometrically nonlinear beam equation, which is solved with an iterative method. The solution is then compared to a parabolic description using a coordinate system centered at the middle of an off-axis parabolic arc. The load required to form a parabolic section as well as the accuracy of such a solution is subsequently derived. The sensitivity of the analytical solution to load uncertainties is considered, which establishes that the method can indeed be realistically implemented on a variety of physical scales. Finally, a novel design implementation and experimental demonstration is described.

2. Mathematical model

Since the deformation of the beam is necessarily large, the analysis uses geometric nonlinearity in the formulation of the beam equation in order to capture a wide range of aperture sizes and large distortions of the beam. Consider the Euler–Bernoulli beam equation (Popov, 1968) used for long slender beams, with geometric nonlinearity included

$$\frac{y''}{(1+y'^2)^{3/2}} = \frac{M}{EI}, \tag{1}$$

where M is the moment in the beam, y is the out of plane displacement, and EI is the bending modulus. This nonlinear differential equation (1) can be solved iteratively. Eq. (1) is reordered as follows:

$$y'' = \frac{M}{EI}(1 + y'^2)^{3/2}. \tag{2}$$

The exponential term on the right side of (2) is expanded in a Taylor series in powers of y'^2. This converges for $y'^2 < 1$.

$$y'' = \frac{M}{EI}\left(1 + \frac{3}{2}y'^2 + \frac{3}{8}y'^4 - \frac{1}{16}y'^6 + \frac{3}{128}y'^8 - \mathrm{O}(y'^{10})\right). \tag{3}$$

Consider the case when the moment M results from a combination of pure moment, transverse shear, and axial load applied at the ends of the beam as shown in Fig. 1.

Due to the deformation of the beam, the axial load produces a nonconstant moment distribution along the beam.

$$M(x) = M_0 - F_x y - F_y x, \tag{4}$$

where the moment at $x = 0$ is M_0 the moment at the direct applied load at the beam end is M_b, the compressive load is F_x and the transverse shear load is F_y.

$$M_0 = M_\mathrm{b} + F_x y_\mathrm{max} + F_y x_\mathrm{max}, \tag{5}$$

and substitute into Eq. (3)

$$\begin{aligned} y'' = {} & \frac{M_0}{EI}\left(1 + \frac{3}{2}y'^2 + \frac{3}{8}y'^4 - \frac{1}{16}y'^6 + \cdots\right) - \frac{F_x}{EI}\left(y + \frac{3}{2}y'^2 y + \frac{3}{8}y'^4 y - \cdots\right) \\ & - \frac{F_y}{EI}\left(x + \frac{3}{2}y'^2 x + \frac{3}{8}y'^4 x + \cdots\right). \end{aligned} \tag{6}$$

In the first iteration the first term only on the right side of Eq. (6) is used, which gives

$$y = \frac{M_0}{EI}\frac{x^2}{2} \quad \text{and} \quad y' = \frac{M_0}{EI}x. \tag{7}$$

Eq. (7) is substituted into Eq. (6) and integrated. After four such iterations

$$\begin{aligned} y = {} & \frac{M_0}{2EI}x^2 - \frac{F_y}{6EI}x^3 + \left(\frac{1}{8}\left(\frac{M_0}{EI}\right)^3 - \frac{1}{24}\frac{F_x}{EI}\frac{M_0}{EI}\right)x^4 + \left(\frac{1}{120}\left(\frac{F_x}{EI}\right)\left(\frac{F_y}{EI}\right) - \frac{3}{20}\left(\frac{M_0}{EI}\right)^2\left(\frac{F_y}{EI}\right)\right)x^5 \\ & + \left(\frac{1}{16}\left(\frac{M_0}{EI}\right)^5 - \frac{11}{240}\frac{F_x}{EI}\left(\frac{M_0}{EI}\right)^3 + \frac{1}{720}\left(\frac{F_x}{EI}\right)^2\frac{M_0}{EI} + \frac{1}{16}\left(\frac{F_y}{EI}\right)^2\frac{M_0}{EI}\right)x^6 + \mathrm{O}(x^7). \end{aligned} \tag{8}$$

Subsequent iterations begin with correction to $\mathrm{O}(x^7)$. When Eq. (8) is inspected for the case of $F_x = 0$ and $F_y = 0$ the Taylor series expansion for a circular arc is obtained which gives a quick check on the solution form.

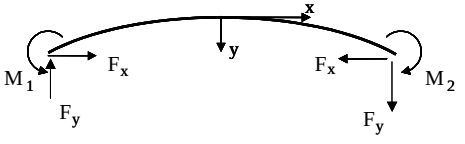

Fig. 1. Beam with moment, shear, and axial compression applied at ends.

2.1. On-axis parabolic deformed shape

Of particular importance is the special case of an on-axis parabola where the vertex is at the center of the beam. In this case the form of the desired shape is simply

$$y = \frac{1}{2R}x^2. \tag{9}$$

The on-axis case by symmetry has $F_y = 0$ which eliminates the odd powers in the polynomial expansion. The optimal load inputs can be selected to balance each other and eliminate selected terms in the polynomial expansion. If by design a compressive load, moment, and transverse shear are selected as design parameters, then the cubic and quartic terms in Eq. (8) can by eliminated and the parabolic term prescribed. Such a balancing is given by

$$F_y = 0, \quad M_0 = \frac{EI}{R}, \quad F_x = \frac{3M_0^2}{EI} \tag{10}$$

The error from parabolic is therefore

$$y_{\text{error}} = -\frac{1}{16}\frac{x^6}{R^5} + \mathrm{O}(x^8). \tag{11}$$

The F-number of the system is defined as $F\# = R/2d$. The corresponding RMS error over the entire length is

$$e_{\text{RMS}} \approx \frac{1}{2^{15}\sqrt{13}}\frac{d}{F\#^5}. \tag{12}$$

Note also that the polynomial expansion for the out of plane deformation can equivalently be written as an expansion in $F\#$ which may be useful in certain cases. Accuracy limit as a function of a aperture size and $F\#$ is shown in Fig. 2.

2.2. Transformation of coordinates

In an optical design, an off-axis parabolic section may be required. In the analysis which follows, the deviation from parabolic which is measured normal to the surface is desired. The polynomial expression is therefore derived for a section of a parabola transformed from a coordinate system located at the parabola vertex to a coordinate system centered at the particular arc of parabola being considered. Fig. 3 shows the detail of the orientation.

The equation of a parabola with coordinate system at the vertex of the parabola is simply

$$y^* = \frac{1}{2R}x^{*^2}, \tag{13}$$

where R is the radius at vertex. The coordinate system translated from O to P, a distance x_0 along the x^* system. A rotation is then applied to a coordinate system tangent to the parabolic arc at P denoted by x and y, where $y_0 = x_0^2/2R$, and $\theta = \tan^{-1}(x_0/R)$.

$$x = (x^* - x_0)\cos\theta + \left(y^* - \frac{x_0^2}{2R}\right)\sin\theta, \tag{14a}$$

$$y = -(x^* - x_0)\sin\theta + \left(y^* - \frac{x_0^2}{2R}\right)\cos\theta, \tag{14b}$$

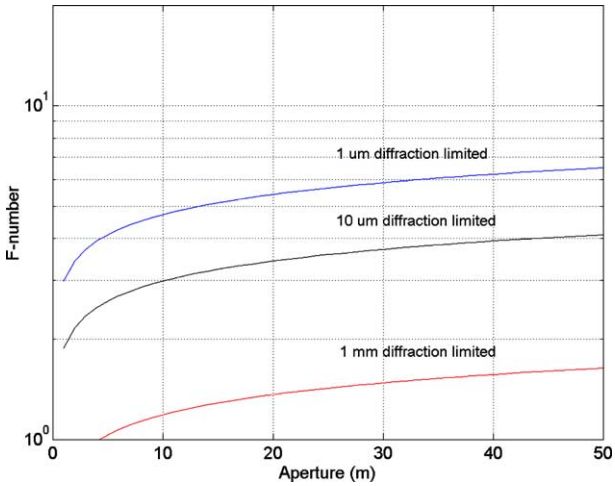

Fig. 2. Accuracy limit of on-axis parabolic shape for diffraction limited performance approximately defined as error$\mathrm{RMS} = \lambda/28$.

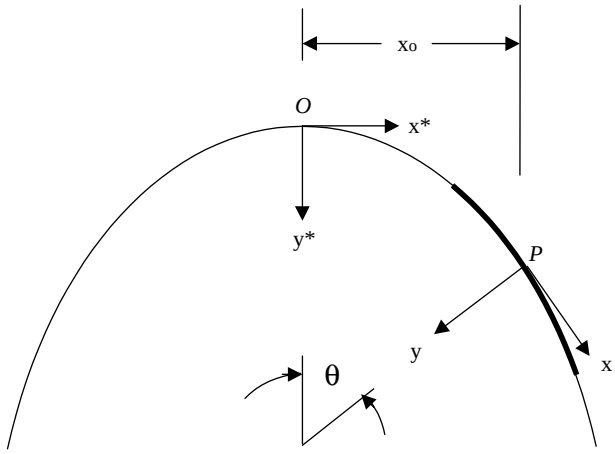

Fig. 3. Off-axis section of a parabola with transformation of coordinate system.

combining Eqs. (13) and (14) and some manipulation gives the equation of the off-axis parabolic section about a coordinate system tangent and centered at the middle of the parabolic section.

$$y = \cos^3\theta\frac{x^2}{2R} - \sin\theta\cos^5\theta\frac{x^3}{2R^2} + \sin^2\theta\cos^7\theta\frac{5x^4}{8R^3} - \sin^3\theta\cos^9\theta\frac{7x^5}{8R^4} + \cdots \mathrm{O}\left(\frac{x^6}{R^5}\right) \tag{15}$$

A comparison of Eqs. (8) and (15) shows that there are again enough degrees of freedom in the loading design to match the first three terms of the polynomial, thus generally producing an off- axis parabolic bent beam with deviation from parabolic error $\mathrm{O}(x^5/R^4)$.

2.3. Off-axis parabolic deformed shape

The equations for the off-axis case were given in Eq. (8). The optimal solution in this case would match the lowest order terms of the power series expansion equation (15). Since there are three loads possible then the first three terms can be matched. The quadratic term is matched for

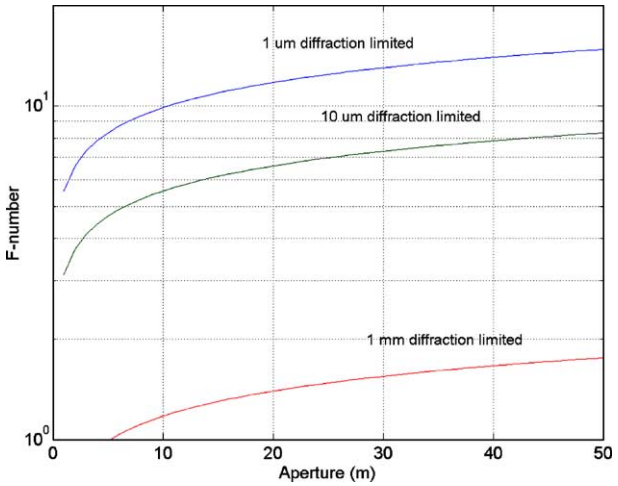

Fig. 4. Accuracy limit of 20° off-axis parabolic shape for diffraction limited performance approximately defined as errorRMS = $\lambda/28$.

$$M_0 = \frac{EI}{R}\cos^3\theta. \tag{16}$$

The cubic term is matched for

$$F_y = -\frac{3EI}{R^2}\sin\theta\cos^5\theta. \tag{17}$$

The quartic term is matched for

$$F_x = \frac{3EI}{R^2}(\cos^6\theta - 5\sin^2\theta\cos^4\theta). \tag{18}$$

Substituting these optimal values into Eq. (8) and comparing to Eq. (15) gives the error from parabolic as being dominated by the x^5 term

$$y_{\text{error}} \approx -\left(\frac{9}{20}\sin\theta\cos^{11}\theta - \frac{27}{32}\sin^3\theta\cos^9\theta\right)\frac{x^5}{R^4} + \cdots \mathrm{O}\left(\frac{x^6}{R^5}\right). \tag{19}$$

The RMS error over the length of the arc is given below, where accuracy limit for an off-axis case is shown in Fig. 4.

$$e_{\text{RMS}} \approx \frac{1}{(2^{11})\sqrt{11}}\left(-\frac{9}{5}\sin\theta\cos^{11}\theta + \frac{27}{8}\sin^3\theta\cos^9\theta\right)\frac{d}{F\#^4}. \tag{20}$$

3. Load sensitivity

The sensitivity of the parabolic shape to deviations in the load pattern from optimal is described by the partial derivative of Eq. (8) with respect to the applied end loads. This calculation bears directly on the feasibility of implementation of the above calculations into real hardware. Unrealistic requirements on the applied load accuracy would indicated a design that is difficult to fabricate and implement.

Taking the derivative of Eq. (8) with respect to the applied moment and force gives the relative sensitivity of each of these loads on the deformed shape. Taking the derivative with respect to the applied moment M_0 and evaluating at the optimal value of balanced loads gives

$$\frac{\partial y}{\partial M_0} = \frac{1}{2EI}x^2 + \frac{M_0^2}{4E^3I^3}x^4 + \mathrm{O}(x^5). \tag{21}$$

This is approximately the same for both the on-axis and off-axis cases of Sections 2.1 and 2.3. Now taking the derivative with respect to the in-line load F_x and evaluating at the optimal load values gives

$$\frac{\partial y}{\partial F_x} = \frac{\cos^3\theta}{24EIR}x^4 + \mathrm{O}\left(\frac{x^5}{R^2}\right). \tag{22}$$

Taking the derivative with respect to the shear load F_y.

$$\frac{\partial y}{\partial F_y} = \frac{1}{6EI}x^3 + \mathrm{O}\left(\frac{x^5}{R^2}\right). \tag{23}$$

The uncertainty in the displacement is linearly related to the uncertainty in the applied loads as shown in Eqs. (21)–(23). Some example calculations of the magnitude and interpretation of these sensitivities is given in the discussion of Section 5.

4. Experiment

A design implementation and experiment is presented to illustrate the simplicity and utility of this method of forming parabolic beams that are accurate to the micrometer and potentially the submicrometer level. The emphasis of the experiment is on the important special case of a parabolic on-axis deformation (Fig. 5).

Examining Eqs. (8) and (10), it is apparent that a compressive load applied at the end of a extension arm with $(L + y_{\max}) = R/3$ will balance the moment and compression giving $F_x = 3M_0/R$ so as to eliminate the quartic term in the polynomial expansion Eq. (8) and give an on-axis parabola with error $\sim x^6/R^5$. This suggests a very simple implementation that requires only one load application, F_x, or equivalently, an applied displacement actuation site between the two extension arms as shown in Fig. 5. These long extension arms may not be practical for a real reflector design, however it is very useful feature in simplifying the

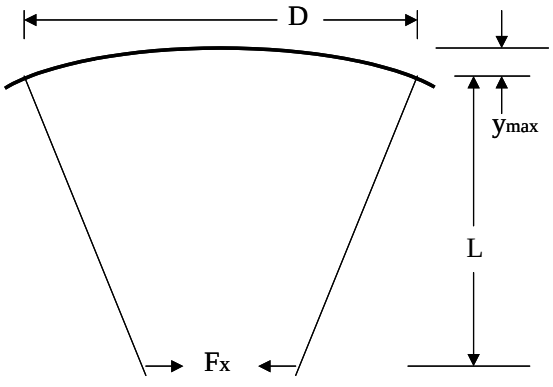

Fig. 5. Geometry and nomenclature for balancing the moment and applied axial compression.

experiment since only one load is directly applied and the balancing of moment and compression is provided by the geometry of the design.

Fig. 6 shows a photo of the experimental implementation of this design. The experimental beam consisted of an off-the-shelf flat aluminum 6061-T6 bar 9.5 mm × 51 mm × 1.83 m long with load extension standoffs fastened 38 mm from each end, giving an effective beam length, D, of 1.75 m. Measurements were taken over the central 1.72 m of this region. The standoffs were made of 0.025 m aluminum 6061-T6 tube. The tube were 1.7 m long and at their end had a hole drilled that allow a threaded bar to pass between them. Adjusting the threaded bar effectively pulled the two extension standoffs together, thereby applying a balanced compression and moment to the shaping beam as described previously. The entire assembly was suspended 10 feet from the ceiling at four (corners) and hung horizontally as shown in Fig. 6 in order to avoid friction contact effects with the reference table. Measurements on the beam surface were made before and after the threaded bar was adjusted, thus representing the initial undeformed state and the deformed state. For the deformed state, the threaded bar was adjusted until the max deformation of the beam was the prescribed value. The off-the-shelf beam had some initial measurable deformation which was subsequently subtracted from the measured deformed state during the parabolic fit calculations. Measurements on the surface of the beam were corrected using local slope measurements to represent the centerline of the beam. The assembly and measurement of the setup was repeated on two consecutive days and parabolic error results varied between the two measurements by about 6%. Measurements of the beam surface spatial coordinates were made using a Leica LTD500 laser tracker. The expected error of individual laser tracker measurements is ≈35 μm. Approximately 800 measurement points were taken along the beam length for shape.

Measurements of error from parabolic for each data point is shown in Fig. 7. The RMS error is 21 μm and exhibits mostly measurement noise. This is a positive result since it means that the beam error from

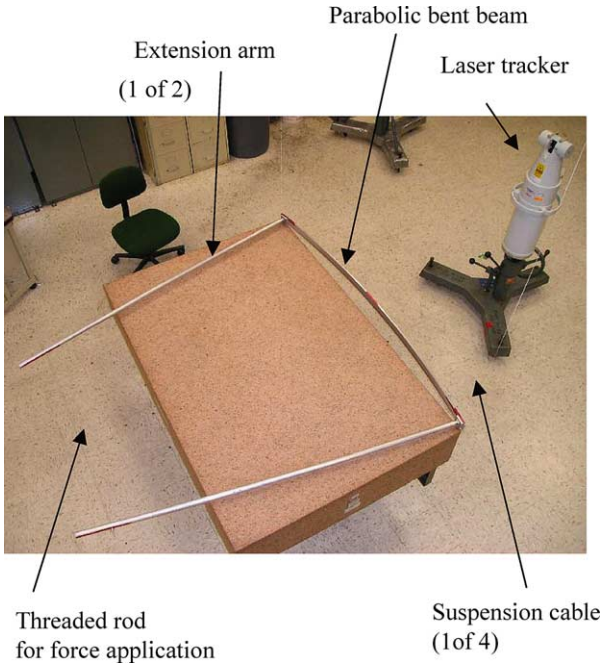

Fig. 6. Photo of the experimental hardware taken from above the setup. The hardware is suspended above a granite reference table. The total deformed beam length is 1.88 m long.

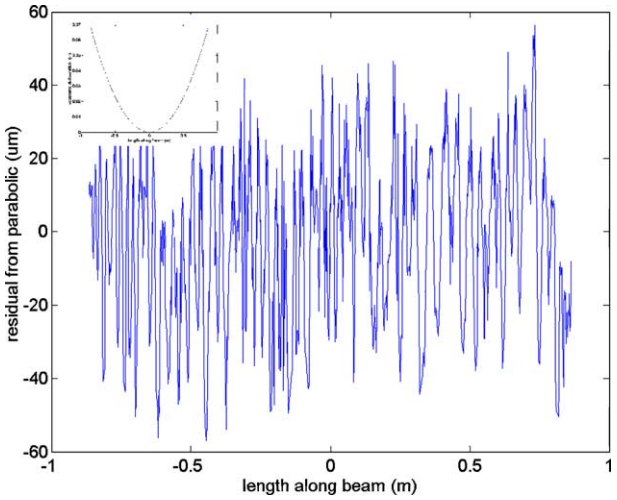

Fig. 7. Error from best fit parabola for each data point. Inset plot shows the parabolic shape of the data.

parabolic is less that this. For comparison, the error from best fit circular shape is 50 μm with characteristic "M" residual shape as expected (not shown), so the balanced forcing was having a significant effect. It is assumed that the beam error from parabolic will have a slow spatial variation so that most of the error shown in the chart is likely the expected 35 μm laser tracker noise. Fig. 7 shows the result where the assumption is made that the short special variation is measurement noise and can be averaged. In Fig. 8 the error data is best fit to a 6th order polynomial where this gives an new estimate of the RMS error of 6.6 μm with a max error of 25 μm.

One source of error that dominates the experimental system was in the initial setup of the hardware. Sag at the beam center was the method of applying a balanced load system on the beam ends. It was not recognized during the setup that this required a precise measure of sag. A standard fine scale was used to measure sag, with an estimated error of ≈1/16 in. or 1.5 mm. What was consequently achieved in the experimental system was a radius at vertex of 5.461 m, not the intended 5.258 m. This curvature radius indicates that the load moment and compression were not balanced exactly. Using the relationship that $M/EI = 1/R$ and $F_x = M/69.0$ for the setup, then one can return to Eq. (8) and find the predicted error from parabola at this radius. The maximum error for the experimental setup was therefore predicted to be 17 μm and the RMS is 5.5 μm, which is in very good agreement with the measured results. The predicted error from parabolic for an ideally balanced load and moment was 7.1 μm max and RMS of 2.1 μm. However, given the measured radius at vertex value, the experiment correlates very well with prediction and points the sort of sensitivity of the parabolic shape errors to hardware implementation errors. In retrospect, the sensitivity to sag measurement is exactly the focus sensitivity that was shown in Eq. (21), and could have been expected to be a parameter that needed to be controlled very well. However, the small degradation of the RMS error from best parabolic fit that was achieved with this rather course setup is evidence of the relative insensitive nature to generally forming a parabolic shape using the method described in this paper. Table 1 gives a comparison of the experimental values of measured beam deformation with the predicted parabolic values of Eqs. (21) and (22).

Other sources of implementation error stem from geometric tolerance error and initial deformation. In particular, the compliance of the standoffs was not included in the calculations for the necessary length of the standoffs. Since this is a nonlinear geometric problem, it is the deformed state of the structure that is required to have standoff length of $R/3$. However, it is easy to show that this results in negligible change

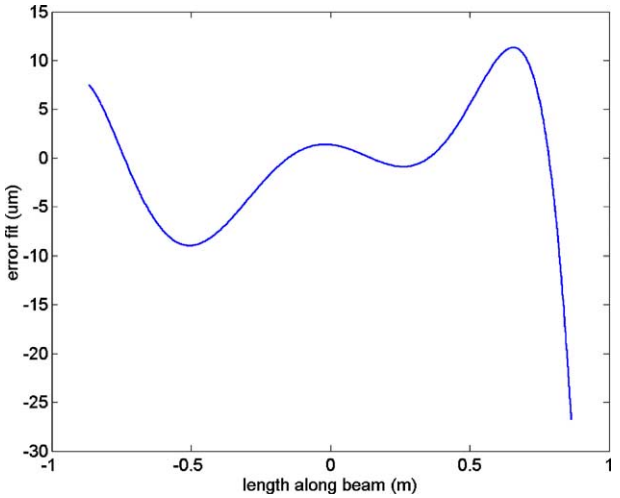

Fig. 8. Error from best fit parabola to a 6th order polynomial curve fit on the data. This averages the small scale spatial variation in data that is assumed to be measurement error of the laser tracker.

Table 1
Comparison of experimental deformation and predicted parabolic shape

	Prediction	Experiment
D Beam length (m)	*Prescribed*	1.753
$F/\#$ ($R/2D$)	*Prescribed*	1.5
y_{max} (m)	*Prescribed*	7.03e−2
L Extension arm length (m)	*Prescribed*	1.680
y_{error} max from parabolic (m)	17.0e−6	25e−6
y_{error} rms from parabolic (m)	5.5e−6	6.6e−6

in the expected deformation. Similarly, there is some small mapping error of initial deformation when subtracting from the final deformed state since the length along the beam is not aligned with the coordinate system in the geometric nonlinear case. Again, this is a negligible effect for the geometries considered here. There is some evidence of anti-symmetry in the error plot of Fig. 8 which is unexpected for the on-axis case and indicates that some direct shear is leaking into the system or that the beam center is not exactly the parabola vertex. The source of this may be assembly tolerance at the standoff fasteners, but this is not clear.

5. Discussion

The ability of a bent beam to form a highly accurate parabolic arc was given in Eqs. (12) and (20) for the cases of an on-axis and off-axis parabola respectively and demonstrated in the experiment of Section 4. Figs. 2 and 4 give graphical representation of these equations for parabolic accuracy. The predicted error from parabolic is essentially a power series in $F/\#$ of the aperture, which is the measure of the radius of curvature to the overall length of the beam. It is more difficult to achieve accurate parabolic shape for long beams and small radius of curvature. Also, it is more difficult to achieve off-axis shapes rather than symmetric on-axis shapes as seen by comparing the two graphs in Figs. 2 and 4. With these considerations, this method of bending beams is theoretically and experimentally demonstrated to be a very effective means of achieving parabolic figure. It may be used for very large apertures, >10 m, as well as application to very

small wavelength electromagnetic waves, into the visible, with reasonable $F/\#$ achieved. The power of the implementation is that it provides a path for cost effective large membrane apertures, since machining and polishing can take place on a flat constant cross section member that is then bent to curvature. For example, a 10 m on-axis aperture Mid-IR telescope system could potentially be formed at $F/4$. Similarly for larger wavelengths, such as RF antenna applications, an $F/1.2$ 10 m system could be built at 100 GHz.

The effect of load uncertainty has been quantified, as given in Eqs. (21)–(23) on the practical aspect of implementing the bend to parabolic technique. For practical dimensions and material properties the loading accuracy required is feasible. Radius of curvature or focal length error is the most sensitive component of the geometry. However, in deriving and designing for the load sensitivity calculations, it is useful to eliminate that portion of the error that produces purely focus error. The reason for this is the corrective lens system or detector should have some capability to actively adjust for focal length. The portion of error that contributes to wavefront error is of greatest concern. For example, consider a 10 m on-axis aperture at $F/3$ to be used at 10 μm wavelength. The RMS deviation from parabolic is about 0.35 μm. Assuming a flat rail that is 0.025 m depth and 0.1 m wide with modulus $E = 200$ GPa, then the moment required to produce this curvature is $M_0 = 434$ N m while and the complementary balancing force to produce parabolic shape is $F_x = 21.7$ N. An uncertainty in the moment, M_0, produces primarily a change in focal length in direct proportion. A 1 N m uncertainty in M_0 produces a focal length change of about 14 cm. This is large, but depends on the focal plane mechanism. In general, focus errors are more easily corrected than higher order errors. If the focal length error represented by the first term in the expansion equation (21) is excluded and only higher order error is considered, then 1 N m uncertainty produces about 0.5 μm RMS of error from parabolic. In terms of RMS error about 0.5 N m of error in the moment application can be neglected. Meanwhile a 1 N uncertainty in F_x from Eq. (22) produces approximately 5 μm RMS of deformation from parabolic over the length. Therefore F_x probably needs to be controlled to about 0.1 N in order for the error to be negligible. These are small numbers but are certainly feasible.

Potential sources of error in the forming of parabolic beams come as errors from simplifying assumptions in the theoretical derivation, as well as implementation errors. A discussion of implementation error for the example experiment was previously given in Section 4 and pointed to the relative insensitivity and slow error growth due to geometry errors in the hardware. Foremost in the derivation errors is the neglect of shear deformation. For the on-axis case very little direct shear is applied to the beam. Shear appears due to the geometric nonlinearity and the compressive load. This introduces a moment distribution in the beam that is approximately two orders of magnitude smaller than the distortion due to the direct constant moment application with a similar result for the off-axis design where some shear is added directly to the beam end. In addition, the beams envisioned for this application and used in our prototypes to date, are long and thin with slenderness ratios of 100–1000. Considering that beam shear deformation goes as the square of the slenderness ratio as well as the small magnitude of the shear load in comparison to the moment applications, then shear deformation is expected to be at lease 6 orders of magnitude smaller than the center sag displacement of the beam. For moderate length beams in the 1–10 m range and small electromagnetic wavelengths, this is still negligible.

6. Conclusions

The potential of a flat beam to be actively bent into an optically accurate parabolic arc was derived analytically and demonstrated experimentally. The error from parabolic was shown to be a function of $F/\#$ where reasonable geometries give very accurate parabolic shape using a simple set of end moments and loads. The sensitivities of the parabolic shape to uncertainties in the load application were derived and it was shown that the required loads are achievable in a lab environment for realistic and desirable telescope and antenna geometry.

References

Ash, J., Jenkins, C., Marker, D., 2000. Design of a membrane mirror using a center plunger. Proceedings of AIAA 4, 174.

Burge, J.H., Cuerden, B., Angel, J.R.P., 2000. Active mirror technology for large space telescopes. Proceedings of SPIE 4013, 640.

Dimakov, S.A., Bogdanov, M.P., Gorlanov, A.V., Kislitsyn, B.V., Zhuk, D.I., 2000. Control of membrane mirror profile by electrostatic field. Proceeding of SPIE 4091, 137.

Dragovan, 2002. DART system for farIR/submillimeter space telescopes. Proceeding of SPIE 4849, 1.

Jenkins, C.H., Wilkes, J.M., Marker, D.K., 1998. Improved surface accuracy of precision membrane reflectors through adaptive rim control. Proceedings of AIAA, 2302.

Popov, E.P., 1968. Introduction to Mechanics of Solids. Prentice-Hall, Englewood Cliffs, NJ, p. 382.

Rotge, J.R., Dass, S.C., Marker, D.K., Carreras, R.A., Lutz, B., Duneman, D.C., 2000. Progress toward large aperture membrane mirrors. Proceedings of SPIE 4091, 74.

Tolomeo, J.A., Cross, G., Sable, B., Decker, T., Putnam, D., Jamieson, T., Dragovan, M., Chmielewski, A., Dooley, J., 2002. Design and test of a prototype DART system. Proceedings of SPIE 4849, 8.

White, C., Salama, M., Dragovan, M., Hatheway, A., Schroeder, J., Dooley, J., Barber, D., 2003. Shaping of parabolic cylindrical membrane reflectors for the DART precision test-bed. Proceedings of AIAA 3, 2288.